

Journal of Materials Chemistry A

Accepted Manuscript



This is an *Accepted Manuscript*, which has been through the Royal Society of Chemistry peer review process and has been accepted for publication.

Accepted Manuscripts are published online shortly after acceptance, before technical editing, formatting and proof reading. Using this free service, authors can make their results available to the community, in citable form, before we publish the edited article. We will replace this *Accepted Manuscript* with the edited and formatted *Advance Article* as soon as it is available.

You can find more information about *Accepted Manuscripts* in the [Information for Authors](#).

Please note that technical editing may introduce minor changes to the text and/or graphics, which may alter content. The journal's standard [Terms & Conditions](#) and the [Ethical guidelines](#) still apply. In no event shall the Royal Society of Chemistry be held responsible for any errors or omissions in this *Accepted Manuscript* or any consequences arising from the use of any information it contains.



Journal Name

ARTICLE

A superior low-cost amorphous carbon anode made from pitch and lignin for sodium-ion batteries

Yunming Li, Yong-Sheng Hu*, Hong Li, Liquan Chen and Xuejie Huang

Received 00th January 20xx,
Accepted 00th January 20xx

DOI: 10.1039/x0xx00000x

www.rsc.org/

Sodium-ion batteries (SIBs) are a promising candidate for grid electricity storage due to the potential low cost. The development of anode materials is a crucial step to promote the commercialization of SIBs, amorphous carbon materials are likely to be the most promising alternative among all proposed anode materials. However, the cost of the reported carbon materials is still very high due to the expensive precursors and their low carbon yield. Here, we reported an amorphous carbon (AC) material made from low cost pitch. The amorphous carbon material with an amazing high carbon yield of 57% was achieved by utilizing the emulsification interaction between pitch and lignin to suppress the graphitization of pitch during the carbonization. The effects of heat-treatment temperatures and the pitch/lignin mass ratios on morphology, microstructure and the electrochemical performance of AC were systematically investigated. By optimizing experimental conditions, we achieved one representative AC with suitable morphology and microstructure, which exhibits promising performances with a high reversible capacity of 254 mAh g⁻¹, a high initial Coulombic efficiency of 82% and excellent cycling stability. This is the first demonstration that the pitch can be successfully applied in fabricating amorphous carbon anode materials for SIBs with superior low cost and high performance.

Introduction

Recently, with the gradual deterioration of ecological environment, the efficient utilization of renewable energy resources has already become an urgent task of creating a healthy eco-environment and sustainable energy structure. The development of low-cost and high-performance energy storage systems (EESs) is an indispensable component for guaranteeing the stable and continuous energy supply. Among secondary batteries, lithium-ion batteries (LIBs), which have been successfully developed as power sources for portable electronics, are a promising alternative source due to their highest energy/power density and long cycle life.¹ However, the rarity and non-uniform geographic distribution of lithium resources may severely restrict LIBs' perspective applications in grid-scale energy storage.^{2,3} Sodium-ion batteries (SIBs) have recently been considered as an alternative energy storage technology to LIBs due to their potentially low-cost and the widespread reserves of sodium resources.⁴⁻⁸

Up to now, a number of cathode materials have been proposed, enabling it possible to produce high-performance SIBs. They mainly include layered oxides (P2 and O3),⁹⁻¹³ tunnel-type oxides,^{14,15} phosphates^{16,17} and sulphates¹⁸. Recently, Hu et al. reported air-stable copper-based P2-

Na_{7/9}Cu_{2/9}Fe_{1/9}Mn_{2/3}O₂ and O3-Na_{0.9}[Cu_{0.22}Fe_{0.30}Mn_{0.48}]O₂, which show very promising application in rechargeable batteries with only environmentally-friendly and low-cost elements.^{19,20}

With respect to anodes, graphite which has been widely used as an anode material for LIBs shows poor Na storage performance due to the unique feature of large and highly ionized Na⁺ ion.²¹ The widely studied anodes for SIBs mainly include carbonaceous materials, alloys²², Ti-based oxides and organic compounds. Na alloy anode materials of Sb/C,²³ Sn/C²⁴ and SnSb/C²⁵ exhibit a high capacity of 610 mAh g⁻¹, 295 mAh g⁻¹ and 540 mAh g⁻¹, respectively. However, the structure destruction caused by the large volume expansion in the reaction with Na limits their cycling stability.²⁶ Ti-based oxides mainly include Na₂Ti₃O₇,²⁷ Li₄Ti₅O₁₂^{28,29} and Na_{0.66}[Li_{0.22}Ti_{0.78}]O₂,³⁰ but either the storage capacity or low Coulombic efficiency hinders their applications. Na₂C₈H₄O₄ is a typical organic compound studied as anode for SIBs, and it delivers a large reversible capacity with good capacity retention.³¹ Nevertheless, insufficient electronic conductivity and low initial Coulombic efficiency limit the further development of organic compounds. Among anode candidates for SIBs, carbonaceous materials hold the most promise considering the resource and cost. Recently, graphite has been studied as a suitable anode for SIBs, the reversible Na insertion and extraction was realized by either enlarging the interlayer distance of graphite or Na⁺-solvent co-intercalation, but the first Coulombic efficiency is very low.³²⁻³⁴ Hard carbon, also known as non-graphitizable carbon, shows promising performances with low operating potential and relatively high specific capacity as anode for SIBs because of its disordered structure with large interlayer distance.³⁵⁻³⁹ Unfortunately, the low initial Coulombic efficiency and the high cost limit its

Key Laboratory for Renewable Energy, Beijing Key Laboratory for New Energy Materials and Devices, Beijing National Laboratory for Condensed Matter Physics, Institute of Physics, Chinese Academy of Sciences, Beijing100190, China. E-mail: yshu@aphy.iphy.ac.cn

† Electronic Supplementary Information (ESI) available: [details of any supplementary information available should be included here]. See DOI: 10.1039/x0xx00000x

application. The poor initial Coulombic efficiency caused by the formation of solid electrolyte interphase (SEI) layer which results in the irreversible loss of Na provided by the cathode would ultimately lead to the capacity decrease in full cell. Hard carbon is usually prepared through pyrolysis of different carbonaceous precursors, such as polymers, sugars, and so on. However, their relatively high cost and low carbon yield (Table 1) give rise to the high cost of hard carbon. Therefore, how to improve the carbon yield and reduce the cost has become a key step to satisfy the requirement for practical application.

As a low-cost petrochemical by-product, pitch is widely used as carbon source for soft carbon and artificial graphite because of the low cost and high carbon content. In 2011, Adelhelm et al. first reported a pitch-derived carbon as anode for SIBs, but it only delivers a storage capacity of about 130 mAh g⁻¹, and the initial Coulombic efficiency is only 14%.⁴⁰ It would be an important breakthrough for the development of low-cost SIBs if we can succeed in fabricating carbonaceous anode materials with high performance using pitch as the precursor. Our very recent work reported the amorphous carbon anode from pitch and phenolic resin, but phenolic resin is expensive (Table 1).⁴¹ Lignin, the second most abundant organic in nature, is a very suitable hard carbon precursor with the features of low cost and abundant. Furthermore, lignin is water soluble and can emulsify pitch, which means that they can crosslink with each other. Herein, we aim to use the pitch as precursor to obtain an amorphous carbon (AC) material with low cost and high carbon yield by using the emulsification interaction between pitch and lignin to suppress the graphitization of pitch in the process of high temperature carbonization. Ultimately, an amorphous carbon material was successfully obtained through pyrolysis of such a mixture of pitch and lignin. When evaluated as an anode for SIBs, the pitch/lignin derived carbon exhibits a high Coulombic efficiency, a relatively high storage capacity and stable cycling performance. It turns out that we introduced an effective strategy to use pitch to prepare amorphous carbon with superior low cost and excellent electrochemical performance, and the method is also suitable for industrial production for its simplicity and high carbon yield.

Table 1 The price and carbon yield at 1000 °C of precursors for amorphous carbon.

Precursor	Pitch	Sucrose	Lignin	Phenolic resin	Starch	Cellulose
Price (\$/ton)	300	400	450	2000	500	1000
Carbon yield (%)	56	<10	43	47	<10	<10

<http://www.alibaba.com/>

Experimental

Materials synthesis

AC was prepared by pyrolysis of the mixture of pitch and lignin. The precursor materials of pitch and lignin (Ourchem Co. China, 96%) with different proportions were mixed in aqueous solutions by ball-milling dispersion method, then the slurry was dried at 100 °C for 24h to remove the water. The obtained black powder was carbonized for 2 hours in a tube furnace

under Argon flow. The carbonization temperatures were 1200 °C, 1400 °C and 1600 °C, respectively. The fabricated amorphous carbon materials denoted as AC111200, AC111400, AC111600, AC731400 and AC371400 were prepared as summarized in Table 2.

Materials characterizations

The structure was characterized by an X'Pert Pro MPD X-ray diffractometer (XRD) (Philips, Netherlands) using Cu-K α radiation (1.5405 Å) and Raman spectra (JY-HR 800). The morphologies of the samples were investigated with a scanning electron microscope (SEM) (Hitachi S-4800). High-resolution transmission electron microscope (HRTEM) and selected area electron diffraction (SAED) patterns were recorded on a FEI Tecnai F20 transmission electron microscope. TGA data were obtained using a NETZSCH STA 409 PC Luxx simultaneous thermal analyser (Germany) from room temperature to 1000 °C at a heating rate of 5 °C min⁻¹ under a nitrogen gas atmosphere. Nitrogen adsorption and desorption isotherms were determined by nitrogen physisorption on a Micromeritics ASAP 2020 analyzer.

Electrochemical measurements

All the electrochemical tests were conducted in coin cells (CR2032). The working electrode was prepared by spreading the mixed slurry of active material and sodium alginate binder in water solvent with a weight ratio of 9.5:0.5 onto Al foil, then dried at 100 °C in vacuum for 10 hours. The electrolyte was a solution of 0.6 M NaPF₆ in ethylene carbonate (EC) and dimethyl carbonate (DMC) (1:1 in volume). A sodium foil was used as the counter electrode and glass fiber was used as the separator. All the operations were operated in the Argon-filled glove box. The discharge and charge tests were carried out on a Land BT2000 battery test system (Wuhan, China) in a voltage range of -0.01–2 V at various C-rates under room temperature. A sodium-ion full cell was constructed using AC111400 sample as the anode and O3-Na_{0.9}[Cu_{0.22}Fe_{0.30}Mn_{0.48}]O₂ as the cathode in a CR2032 coin-type cell. Synthesis method of the Na_{0.9}[Cu_{0.22}Fe_{0.30}Mn_{0.48}]O₂ material was a conventional solid state reaction²⁰. The weight ratio of the two electrodes (anode/cathode) was 1:2.65. The full cells were charged and discharged in a voltage range of 1–4.06 V at 0.2C current rate. The energy density was calculated by dividing the discharge energy value by the total mass of cathode and anode materials.

Results and discussion

It is interesting to find that the lignin can emulsify pitch. We first mixed pitch with lignin in aqueous solutions to make them fully interact with each other before the carbonization process. The mixture solutions containing various pitch/lignin mass ratios of 7/3, 1/1 and 3/7 were prepared considering the disordered degree and carbon yield of amorphous carbon. The microstructure of amorphous carbon may have a remarkable effect on Na storage behavior, ultimately determining the electrochemical performance of carbonaceous anode materials for SIBs. Therefore, we also prepared amorphous

Journal Name

ARTICLE

Table 2 Physical parameters and electrochemical properties for different AC.

Sample	AC111200	AC111400	AC111600	AC731400	AC371400	pitch
Pitch/Lignin	1/1	1/1	1/1	7/3	3/7	0
HTTs ^a (°C)	1200	1400	1600	1400	1400	1400
d_{002} (Å)	3.84	3.61	3.52	3.57	3.66	3.45
L_c (nm)	1.64	2.14	2.86	2.52	1.92	7.39
L_a (nm)	4.13	4.00	3.78	4.09	3.73	5.53
S_{BET} (m ² g ⁻¹)	4.29	1.34	4.55	1.74	34.74	2.85
ICC ^b (mAh g ⁻¹)	247	254	205	200	246	85
CPP ^c (%)	60	65	71	62	70	0
ICE ^d (%)	82	82	75	78	74	58

a The heat treatment temperatures.

b The initial charge capacity.

c The capacity percentage of the plateau region.

d The initial Coulombic efficiency.

carbon materials with different heat-treatment temperatures (HTTs) to investigate the influence of carbonized temperature on carbon structure ordering and electrochemical

performance. Finally, five representative amorphous carbon materials with different degrees of carbon structure ordering were obtained and compared.

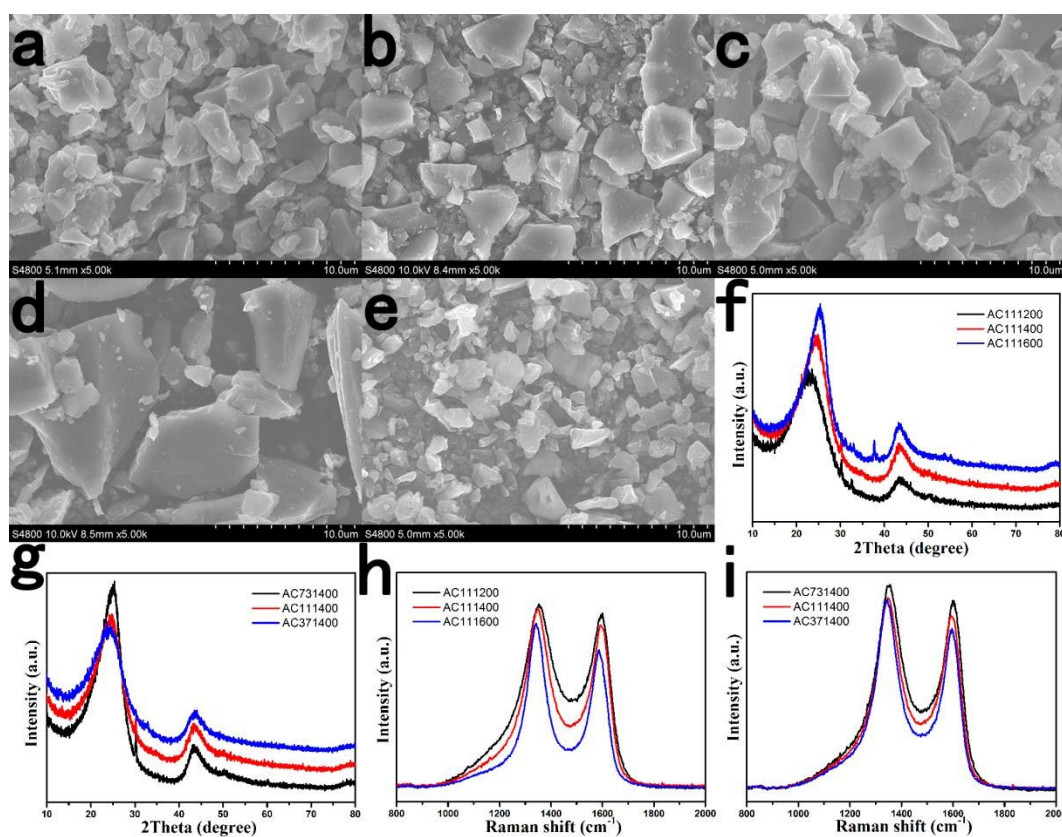


Fig. 1 Morphologies of (a) AC111200, (b) AC111400, (c) AC111600, (d) AC731400 and (e) AC371400 observed by SEM; (f, g) XRD data and (h, i) Raman spectra of AC with different conditions.

The morphologies of AC with various conditions are shown in Fig. 1a-e. All pitch/lignin derived carbon materials are found to be granular morphology with 2-10 μm in size, and non-uniform distribution of the particle size is noted. The particle grows up gradually and becomes uniform and regular with increasing HTTs from 1200 to 1600°C. With increasing addition of lignin content, the morphology becomes from flake to granular and the particle size decreases, which indicates that the lignin is beneficial to restrain the growth of AC.

The microstructure of AC is further characterized by the X-ray diffraction (XRD) and Raman spectroscopy, and the results are shown in Fig. 1f-i. All XRD patterns show the broad peaks at 24° and 43°, which are attributed to the crystallographic planes of (002) and (100) in the disordered carbon structure. The (002) peak position shifts a higher angle and peak becomes narrower with increasing HTTs, indicating d_{002} decreases and L_c increases due to the structural development from disordering to short-range ordering at higher HTTs. In addition, the average interplanar spacing d_{002} increases with decreasing mass ratios of pitch to lignin, suggesting that lignin addition introduces a large amount of topological defects to the AC. Raman spectra present two separate characteristic bands of D-band peak at 1343 cm^{-1} (the defect-induced band) and G-band peak at 1589 cm^{-1} (the

crystalline graphite band).⁴² The half width at half maximum (HWHM) of G and D bands in the Raman spectra decreases slightly with increasing HTTs, which indicates the development of an ordered hexagonal structure. Furthermore, the AC carbonized at higher temperature has a smaller L_a that is calculated from the intensity ratio of D-band over G-band (I_D/I_G), suggesting the (100) direction of small graphitic crystals shrinks at a higher temperature during carbonization process, which may be caused by the curve of graphite layers. We can also find that the value of L_a decreases with the increase of lignin content, which further validates the inhibitory effect of lignin on the crystallization of AC. The results of the XRD and Raman spectroscopy analysis are shown in Table 2.

Fig. 2 shows HRTEM images of different AC. There is no obvious long-range ordered structure in all AC, revealing an amorphous nature of AC, which stands in sharp contrast to the highly-perfect graphitization structure of pitch derived carbon (Fig. 2f). With the increase of carbonization temperature, the locally ordered structure develops further in a random direction over the entire area, especially for AC111600 sample. It is clearly observed with the HRTEM that some parallel carbon hexagonal layers and large numbers of closed voids appear in AC111600 sample, which should be due to the layer shift and fold with respect to each other. All selected area

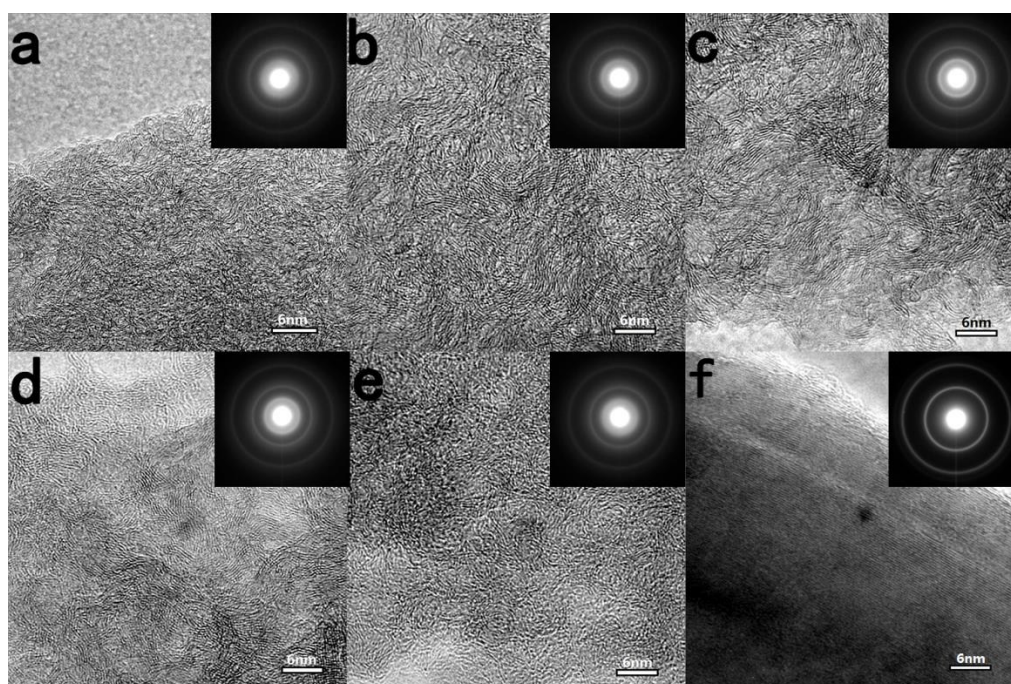


Fig. 2 TEM images and SAED patterns of (a) AC111200, (b) AC111400, (c) AC111600, (d) AC731400, (e) AC371400 and (f) pitch derived carbon with HTTs of 1400°C.

electron diffraction (SAED) patterns show dispersing diffraction rings, which is another demonstration for the amorphous structure of AC. The sharpness of diffraction rings increases with increasing HTTs, a further indication of the development of graphitic structure. Furthermore, with increasing lignin content, the distance between parallel carbon hexagonal layers becomes larger, exhibiting more disordered amorphous structure. That can also be proved by the gradually blurred diffraction rings in SAED patterns. The results of TEM and SAED further demonstrate that the lignin can suppress graphitization and improve the disordered degree of AC, which is favourable for Na storage.

In order to demonstrate that the emulsification interaction between pitch and lignin occurs in the preparation process of AC, we tested the carbon yield of pitch, several kinds of amorphous carbon precursors and the mixture of pitch and them by mean of thermogravimetric analysis (TGA). The results of TGA are presented in Fig. 3a and Fig. S1. The carbon yield of sucrose, lignin and phenolic resin at 1000°C is 7%, 43% and 47%, respectively, while the value of pitch reaches up to 56%. When we mix pitch with sucrose, lignin and phenolic

resin at mass ratio of 1/1, the carbon yield of pitch/sucrose, pitch/lignin and pitch/phenolic resin is 38%, 57% and 52%, respectively. The result indicates that pitch/sucrose and pitch/phenolic resin are just physical mixtures while there is interaction between pitch and lignin in the pitch/lignin mixture. The emulsification interaction between pitch and lignin suppresses the carbon loss of the two in the high-temperature carbonization process, which ultimately results in that the carbon yield of pitch/lignin is even higher than pitch.

FTIR spectra are also applied to evaluate the interaction between pitch and lignin in the pitch/lignin mixture, the result is shown in Fig. 3b. We can see four kinds of chemical bonds owned by both pitch and lignin: OH stretching peak around 3430 cm^{-1} , C-H asymmetric and symmetric stretching of methyl and methylene groups ($2800\text{--}3100\text{ cm}^{-1}$), aromatic skeletal vibrations (1600 and 1458 cm^{-1}) and C-H bending vibration in benzene ring ($670\text{--}870\text{ cm}^{-1}$). It is found that both the C-H stretching peak in methyl and methylene groups at 2840 cm^{-1} and the bending vibration peak in benzene ring at 855 cm^{-1} of lignin move to higher wavenumber in pitch/lignin mixture,

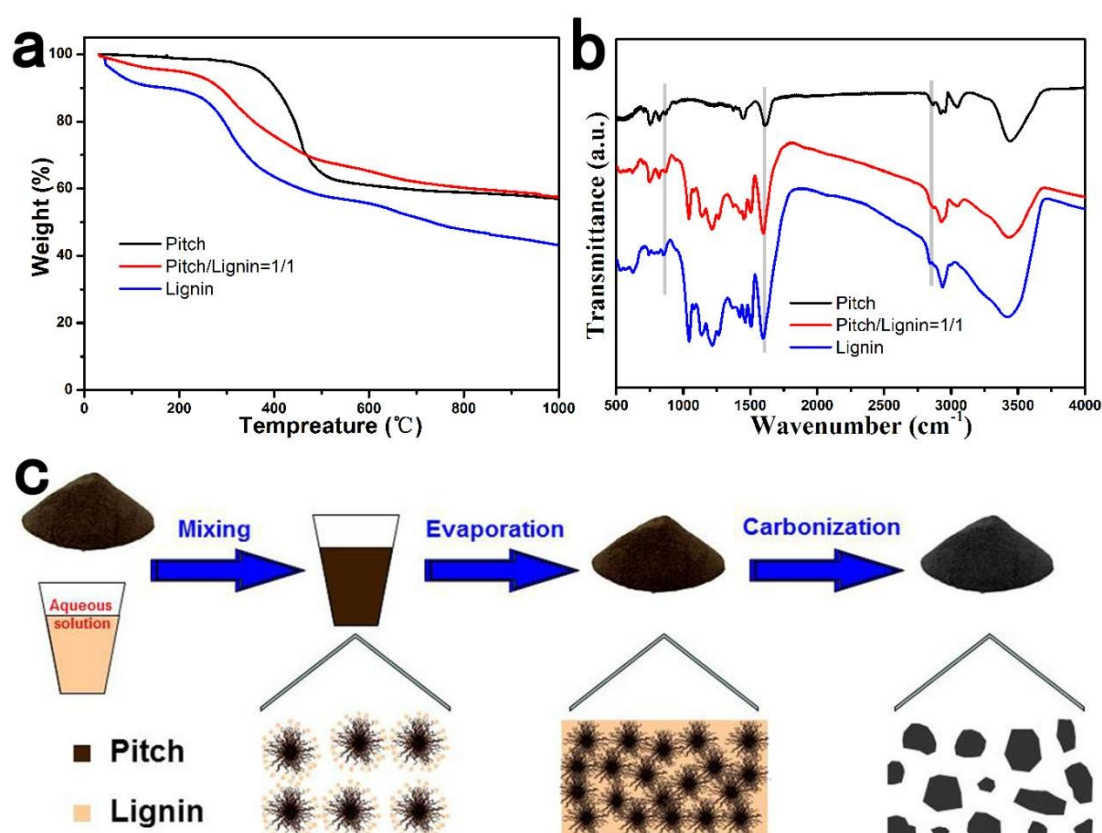


Fig. 3 (a) TGA data and (b) FTIR spectra of pitch, lignin and the mixture of pitch and lignin with weight ratio of 1/1; (c) Principle schematic of the synthesis and proposed mechanism.

which means that the existence of interaction between hydrogen atom of lignin and some atomic groups of pitch leads to the stretching or bending vibration energy increase. This emulsification interaction can also be proved by the movement of aromatic skeletal vibrations peak at 1614 cm^{-1} of pitch to lower wavenumber which is caused by the increase of aromatic skeletal vibration energy. The Fig. 3c presents a schematic of proposed interaction mechanism between pitch and lignin. The clusters of pitch are surrounded by the molecules of lignin and the hydrophilic carboxyl groups arrange outside, thus pitch can be suspended in water forming emulsion with lignin. The result of FTIR spectra successfully proves the existence of the emulsification interaction between pitch and lignin, explaining the TGA result.

The electrochemical properties of AC with different conditions were first investigated using a half-cell test with a sodium foil as counter electrode in order to further understand the influence of material microstructure on Na storage behavior. The first galvanostatic discharge/charge curves at a current rate of 0.1C (30 mA g^{-1}) are shown in Fig. 4a and b. The voltage profiles of all AC electrodes exhibit two distinct regions; 1) a gradual voltage decay around $2.0\text{--}0.115\text{ V}$ and 2) a plateau around 0.1 V . We can see the Na deposition potential at -0.015 V with an obvious turning point (Fig. S3a). The AC111400 sample shows the highest reversible capacity of

254 mAh g^{-1} with a highest initial Coulombic efficiency of 82% which is contributed by the low BET surface areas (Table 2), the capacity percentage of the plateau region is about 65%. For comparison, the pitch derived carbon delivers a very low capacity of 85 mAh g^{-1} with an only sloping voltage profiles (Fig. S2a and Fig. S3b), which is consistent with its highly ordered structure. The reversible capacity and the plateau ratio in overall capacity of AC111200 sample and AC111600 sample are approximately 247 mAh g^{-1} , 60% and 205 mAh g^{-1} , 71%, and the initial Coulombic efficiency of AC111600 sample is as low as 74%. According to previous reports, the slope should correspond to the Na storage in the defect sites, edges and the surface of graphene, and the plateau can be attributed to Na storage in the closed voids.^{43,44} The low capacity of AC111600 sample could be ascribed to the less defects and the higher degree of crystallization which is not beneficial to the Na storage. The large BET surface areas of AC111600 sample significantly increase the formation of SEI, resulting in the lowest initial Coulombic efficiency. As the improvement of HTTs, the decreasing defects are disadvantageous to the storage of Na while the closed voids become relatively advantageous to the Na storage, thus the plateau ratio in overall capacity increases with the increase of carbonized temperature.

The AC anodes with different lignin contents at the same

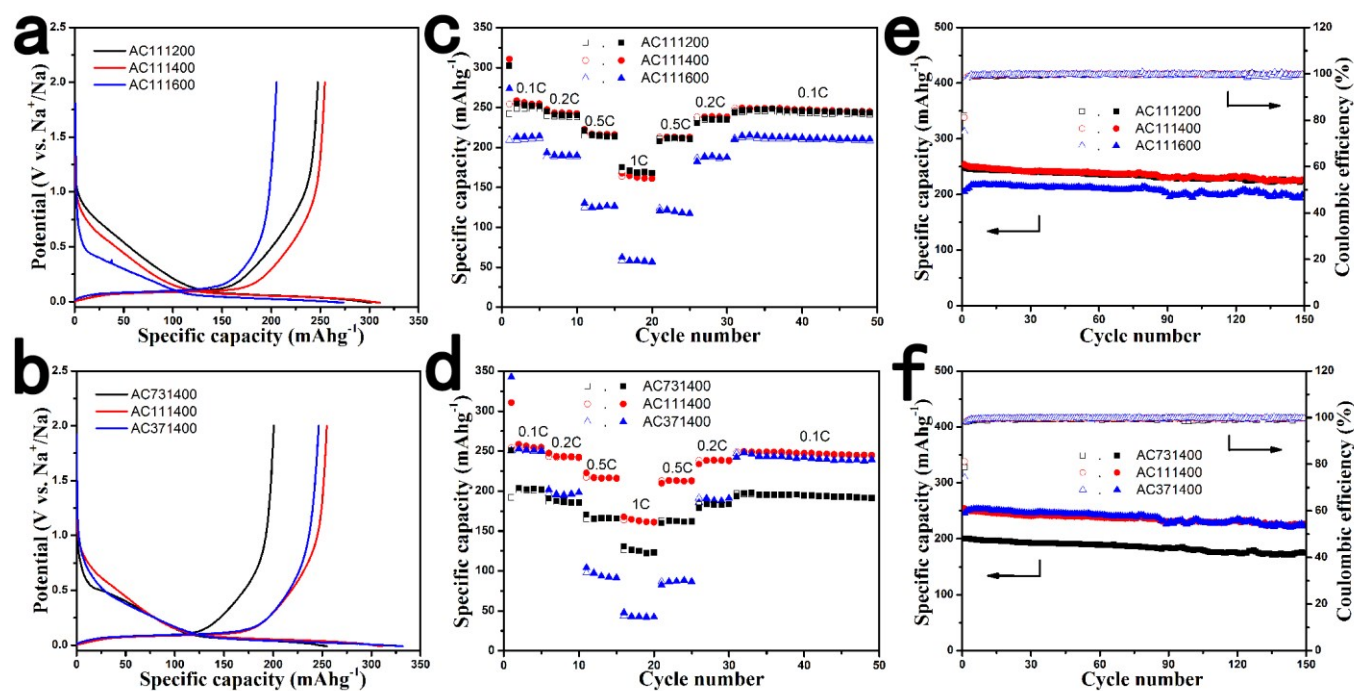


Fig. 4 (a, b) Galvanostatic 1st discharge/charge profiles of all samples at a current rate of 0.1C ; (c, d) Rate capability of all samples from 0.1C to 1C ; (e, f) Cyclic performance of all samples at a current rate of 0.1C .



ARTICLE

HTTs display similar voltage profiles but there are some differences in capacity and the initial Coulombic efficiency. Both AC731400 sample and AC371400 sample are lower than AC111400 sample either in the Na storage capacity or in the initial Coulombic efficiency, which could be attributed to variations of the microstructure. On one hand, the low capacity of AC731400 sample is due to the high graphitization structure reducing available Na storage sites. On the other hand, the large BET surface areas of AC371400 sample induced by increasing the lignin content add irreversible capacity loss. All the above results show that the microstructure of amorphous carbon materials has a significant impact on the Na insertion and extraction capacity. The AC111400 sample exhibits best performance in terms of high reversible capacity and initial Coulombic efficiency as well as cost, which is on account of its appropriate microstructure combining both the defects and the closed voids beneficial to Na storage.

The rate performance of AC electrodes was investigated in detail at various rates from 0.1C to 1C to further identify the effects of HTTs and lignin content on the electrochemical performance, the results are shown in Fig. 4c and d. It can be seen that the rate performance deteriorates with increasing HTTs and the capacity decay at high rate is mainly due to the rapid capacity fading of the plateau region, especially the AC111600 sample. This illustrates that the defect sites are

more favourable for Na⁺ ion transport and the capacity retention of electrodes during large current operation than the closed voids, corresponding to previous reports.⁴⁵ In addition, with the increase of lignin content, the decreasing electronic conductivity resulted from the more disordered graphitization structure is not beneficial to enhancing the rate performance of carbonaceous anode materials. Considering both electronic conductivity and ionic conductivity, the AC111400 sample shows outstanding rate performance with specific capacities of 212 mAh g⁻¹ and 162 mAh g⁻¹ at 0.5C and 1C, respectively. The capacity can return to the previous values when the current rate is reduced, suggesting a good stability of AC under a wide current range.

Fig. 4e and f show the cycling performance of AC with different conditions at 0.1C for 150 cycles. All five amorphous carbon materials have comparable cycling stability, indicating that the lignin content and carbonization temperature do not significantly impact the cycling performance. The AC111400 sample retains a capacity of 226 mAh g⁻¹ after 150 cycles corresponding to a capacity retention of 89%, and the Coulombic efficiencies can keep nearly 100% after the first few cycles. Such excellent cycling performance is most likely due to good mechanical properties and high electronic conductivity of the unique amorphous carbon material.

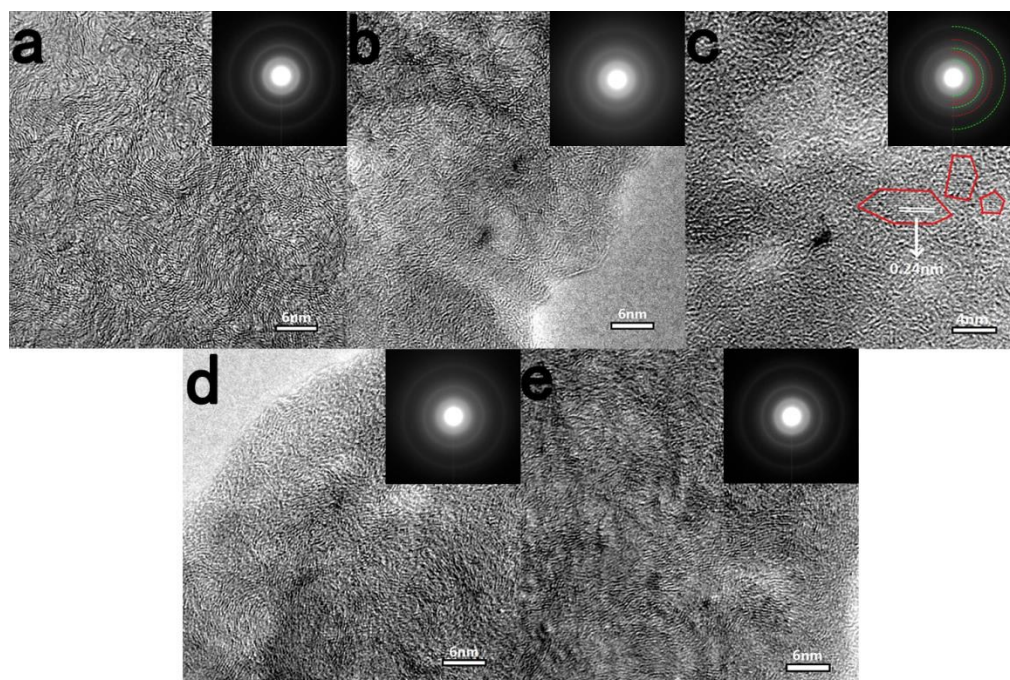


Fig. 5 Ex situ TEM images and SAED patterns of AC111400. (a) Pristine sample; (b) After discharging to 0.115V; (c) After discharging to -0.01V, green and red semicircles represent the diffraction rings from AC and Na metal; (d) After charging to 0.115V; (e) After charging to 2V.

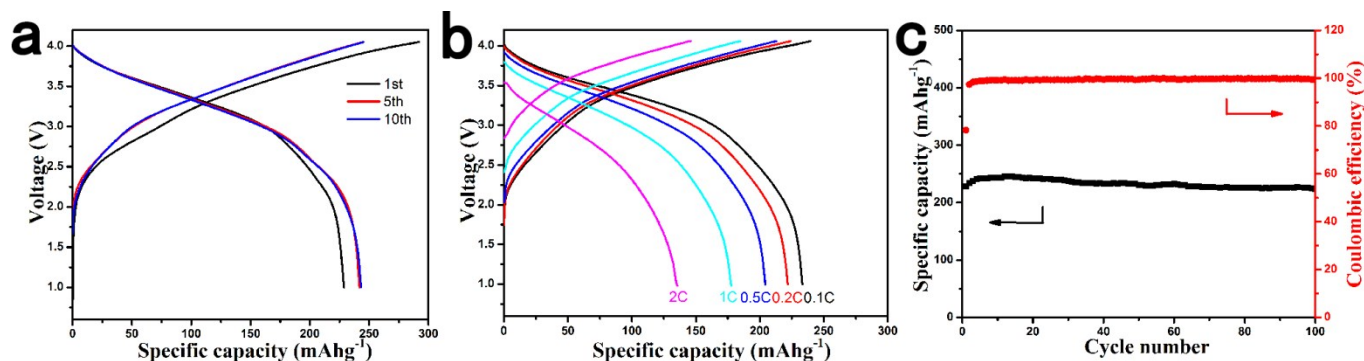


Fig. 6 The performance of a coin-type $\text{Na}_{0.9}[\text{Cu}_{0.22}\text{Fe}_{0.30}\text{Mn}_{0.48}]\text{O}_2/\text{AC111400}$ full cell. (a) Charge and discharge curves for the 1st, 5th and 10th cycles at a current rate of 0.2C; (b) Rate capability at vary constant charge/discharge rates from 0.1C to 2C; (c) Cycling performance at a current rate of 0.2C.

To further deepen the understanding of Na storage mechanism in amorphous carbon materials, we carried out the ex situ TEM experiments using the AC111400 electrode. The structural evolution of amorphous carbon in the discharge/charge progress is shown in Fig. 5. When the AC111400 electrode is discharged to 0.115V which is the cut-off voltage of the sloping capacity, the structure becomes more disordered, indicating the Na storage in the surface of graphene. With further discharged to the final state, several Na metal nanoclusters are directly observed in the TEM image. The SAED in the inset of Fig. 5c also clearly shows the appearance of (110), (111) and (220) crystal planes of Na metal after complete sodiation. Both TEM and SAED demonstrate the Na storage in closed voids of amorphous carbon, and the storage capacity corresponds to the plateau region in electrochemical curves, indicating closed voids provide more energetically stable sodium environments. The result also illustrates why there is no plateau region in the electrochemical curves of pitch derived carbon with highly ordered graphitization structure. The structure of AC111400 sample becomes more disordered after a cycle which ensures the cycling stability in the subsequent electrochemical cycle.

The AC111400 sample was coupled with a cathode of SIBs to demonstrate the application prospects of AC in full cell. The $\text{O3-Na}_{0.9}[\text{Cu}_{0.22}\text{Fe}_{0.30}\text{Mn}_{0.48}]\text{O}_2$ which is designed and prepared by our group for the first time was chosen as the cathode to assemble a full cell.²⁰ The $\text{Na}_{0.9}[\text{Cu}_{0.22}\text{Fe}_{0.30}\text{Mn}_{0.48}]\text{O}_2$ is of particular interest because of the excellent stability in air and even in water, and it is the only stable O3 layered oxide reported by far. In addition, the $\text{Na}_{0.9}[\text{Cu}_{0.22}\text{Fe}_{0.30}\text{Mn}_{0.48}]\text{O}_2$ does not contain toxic and expensive transition metals, which makes it be very suitable for practical application in grid electrical energy storage with only environmentally-friendly and low-cost elements. The Na storage behaviour of

$\text{Na}_{0.9}[\text{Cu}_{0.22}\text{Fe}_{0.30}\text{Mn}_{0.48}]\text{O}_2$ is shown in Fig. S3, the stable cycle performance is achieved with a reversible capacity of 100 mAh g^{-1} at a current density of 10 mA g^{-1} .

The preliminary electrochemical measurement results of full cells with the $\text{Na}_{0.9}[\text{Cu}_{0.22}\text{Fe}_{0.30}\text{Mn}_{0.48}]\text{O}_2$ cathode and the AC111400 anode are displayed in Fig. 6. The $\text{Na}_{0.9}[\text{Cu}_{0.22}\text{Fe}_{0.30}\text{Mn}_{0.48}]\text{O}_2/\text{AC111400}$ full cell delivers a reversible capacity of 240 mAh g^{-1} (based on anode) after several cycle activation, an average operating voltage of 3.2 V and a high initial Coulombic efficiency of 78% at a current rate of 0.2C (60 mA g^{-1}). Even at a current rate of 1C, the full cell can still deliver approximately 177 mAh g^{-1} . A superior cycle performance is shown in Fig. 6c with a capacity retention of 97% after 100 cycles. The energy density of this system is calculated to be 207 Wh/kg . In addition, to further reduce the cost and improve the energy density of the full cell, we used the cheaper and lighter Al foil instead of Cu foil as current collector. A more environmentally benign aqueous sodium alginate binder was also used to reduce the environmental pollution brought by this system.

Conclusions

This work reported a novel high yielding and low-cost amorphous carbon anode material from pitch with an adjustable microstructure for sodium-ion batteries. Several amorphous carbon materials were first successfully fabricated from a mixture of pitch and lignin, then the Na storage behaviour was investigated. The results of TGA and FTIR show that there is emulsification interaction between pitch and lignin, resulting in the extraordinary high carbon yield of 57%. The microstructure of AC varies with the variation of HTTs and the mass ratios of pitch to lignin, which leads to different electrochemical performances in SIBs depending on the

defects and the closed voids. Among all AC, the AC111400 sample shows the best overall performances with a reversible capacity of 254 mAh g⁻¹, a high initial Coulombic efficiency of 82% and good rate performance. The practical feasibility of AC111400 sample in full cell was further confirmed by combining with an air-stable O₃-Na_{0.9}[Cu_{0.22}Fe_{0.30}Mn_{0.48}]O₂ cathode, delivering an energy density of 207 Wh kg⁻¹ and excellent cycling stability with a capacity retention of 97% after 100 cycles. The results of this study show that tailoring carbon microstructure is a critical factor for tuning the electrochemical performance of carbonaceous anode materials of SIBs. This work not only reports a superior low-cost amorphous carbon anode for SIBs with a promising application prospect but also offers a strategy for various electrode materials design in the future.

Author contributions

Y.-S. H. conceived and designed this work; Y. M. L. performed all the synthesis and electrochemical experiments; Y. M. L. and Y.-S. H. wrote the paper; all the authors participated in analysis of the experimental data and discussions of the results as well as preparing the paper.

Acknowledgements

This work was supported by funding from the NSFC (51222210, 11234013, and 51421002), "973" Projects (2012CB932900), and the One Hundred Talent Project of the Chinese Academy of Sciences.

Notes and references

- 1 M. Armand and J. M. Tarascon, *Nature*, 2008, **451**, 652.
- 2 L. M. Suo, Y.-S. Hu, H. Li, M. Armand, L. Q. Chen, *Nat. Commun.*, 2013, **4**, 1481.
- 3 H. L. Pan, Y.-S. Hu and L. Q. Chen, *Energy Environ. Sci.*, 2013, **6**, 2338–2360.
- 4 J. M. Tarascon, *Nat. Chem.*, 2010, **2**, 510.
- 5 S.-W. Kim, D.-H. Seo, X. Ma, G. Ceder and K. Kang, *Adv. Energy Mater.*, 2012, **2**, 710.
- 6 M. D. Slater, D. Kim, E. Lee, C. S. Johnson, *Adv. Funct. Mater.*, 2013, **23**, 947.
- 7 N. Yabuuchi, K. Kubota, M. Dahbi, and S. Komaba, *Chem. Rev.*, 2014, **114**, 11636.
- 8 S. Yuan, X.-L. Huang, D.-L. Ma, H.-G. Wang, F.-Z. Meng and X.-B. Zhang, *Adv. Mater.*, 2014, **26**, 2273.
- 9 N. Yabuuchi, M. Kajiyama, J. Iwatate, H. Nishikawa, S. Hitomi, R. Okuyama, R. Usui, Y. Yamada, S. Komaba, *Nat. Mater.*, 2012, **11**, 512.
- 10 D. D. Yuan, W. He, F. Pei, F. Y. Wu, Y. Wu, J. F. Qian, Y. L. Cao, X. P. Ai and H. X. Yang, *J. Mater. Chem. A*, 2013, **1**, 3895.
- 11 J. Xu, D. H. Lee, R. J. Clement, X. Yu, M. Leskes, Andrew, J. Pell, G. Pintacuda, X. Q. Yang, C. P. Grey and Y. S. Meng, *Chem. Mater.*, 2014, **26**, 1260.
- 12 P. Vassilaras, A. J. Toumar, G. Ceder, *Electrochem. Commun.*, 2014, **38**, 79.
- 13 H. Yu, S. Guo, Y. Zhu, M. Ishida and H. Zhou, *Chem. Commun.*, 2014, **50**, 457.
- 14 Y. S. Wang, J. Liu, B. Lee, R. M. Qiao, Z. Z. Yang, S. Y. Xu, X. Q. Yu, L. Gu, Y.-S. Hu, W. L. Yang, K. Kang, H. Li, X.-Q. Yang, L. Q. Chen and X. J. Huang, *Nat. Commun.*, 2015, **6**, 6401.
- 15 S. Y. Xu, Y. S. Wang, L. B. Ben, Y. C. Lyu, N. N. Song, Z. Z. Yang, Y. M. Li, L. Q. Mu, H. T. Yang, L. Gu, Y.-S. Hu, H. Li, Z.-H. Cheng, L. Q. Chen and X. J. Huang, *Adv. Energy Mater.*, 2015, doi: 10.1002/aenm.201501156.
- 16 K. T. Lee, T. N. Ramesh, F. Nan, G. Botton and L. F. Nazar, *Chem. Mater.*, 2011, **23**, 3593.
- 17 Z. L. Jian, W. Z. Han, X. Lu, H. X. Yang, Y.-S. Hu, J. Zhou, Z. B. Zhou, J. Q. Li, W. Chen, D. F. Chen and L. Q. Chen, *Adv. Energy Mater.*, 2013, **3**, 156.
- 18 P. Barpanda, G. Oyama, S.-I. Nishimura, S.-C. Chung and A. Yamada, *Nat. Commun.*, 2014, **5**, 4358.
- 19 Y. M. Li, Z. Z. Yang, S. Y. Xu, L. Q. Mu, L. Gu, Y.-S. Hu, H. Li and L. Q. Chen, *Adv. Sci.*, 2015, **2**, 1500031.
- 20 L. Q. Mu, S. Y. Xu, Y. M. Li, Y.-S. Hu, H. Li, L. Q. Chen and X. J. Huang, *Adv. Mater.*, 2015, doi: 10.1002/adma.201502449.
- 21 P. Ge and M. Foulletier, *Solid State Ionics*, 1988, **28**, 1172–1175.
- 22 J. Liu, Y. Wen, P. A. van Aken, J. Maier and Y. Yu, *Nano Lett.*, 2014, **14**, 6387–6392.
- 23 J. F. Qian, Y. Chen, L. Wu, Y. L. Cao, X. P. Ai and H. X. Yang, *Chem. Commun.*, 2012, **48**, 7070.
- 24 Y. H. Xu, Y. J. Zhu, Y. H. Liu and C. S. Wang, *Adv. Energy Mater.*, 2013, **3**, 128.
- 25 L. F. Xiao, Y. L. Cao, J. Xiao, W. Wang, L. Kovarik, Z. M. Nie and J. Liu, *Chem. Commun.*, 2012, **48**, 3321.
- 26 V. L. Chevrier, G. Ceder, *J. Electrochem. Soc.*, 2011, **15**, A1011–A1014.
- 27 H. L. Pan, X. Lu, X. Q. Yu, Y.-S. Hu, H. Li, X. Q. Yang and L. Q. Chen, *Adv. Energy Mater.*, 2013, **3**, 1186.
- 28 Y. Sun, L. Zhao, H. L. Pan, X. Lu, L. Gu, Y.-S. Hu, H. Li, M. Armand, Y. Ikuhara, L. Q. Chen and X. J. Huang, *Nat. Commun.*, 2013, **4**, 1870.
- 29 X. Q. Yu, H. L. Pan, W. Wan, C. Ma, J. M. Bai, Q. P. Meng, S. N. Ehrlich, Y.-S. Hu and X.-Q. Yang, *Nano Lett.*, 2013, **13**, 4721.
- 30 Y. S. Wang, X. Q. Yu, S. Y. Xu, J. M. Bai, R. J. Xiao, Y.-S. Hu, H. Li, X. Q. Yang, L. Q. Chen and X. J. Huang, *Nat. Commun.*, 2013, **4**, 2365.
- 31 L. Zhao, J. M. Zhao, Y. S. Hu, H. Li, Z. B. Zhou, M. Armand and L. Q. Chen, *Adv. Energy Mater.*, 2012, **2**, 962–965.
- 32 Y. Wen, K. He, Y. J. Zhu, F. D. Han, Y. H. Xu, I. Matsuda, Y. Ishii, J. Cumings and C. S. Wang, *Nat. Commun.*, 2014, **5**, 4033.
- 33 B. Jache and P. Adelhelm, *Angew. Chem. Int. Ed.*, 2014, **53**, 10169–10173.
- 34 H. Kim, J. Hong, Y.-U. Park, J. Kim, I. Hwang and K. Kang, *Adv. Funct. Mater.*, 2015, **25**, 534–541.
- 35 D. A. Stevens and J. R. Dahn, *J. Electrochem. Soc.*, 2000, **147**, 1271–1273.
- 36 S. Komaba, W. Murata, T. Ishikawa, N. Yabuuchi, T. Ozeki, T. Nakayama, A. Ogata, K. Gotoh and K. Fujiwara, *Adv. Funct. Mater.*, 2011, **21**, 3859–3867.
- 37 K. Tang, L. J. Fu, R. J. White, L. H. Yu, M. M. Titirici, M. Antonietti and J. Maier, *Adv. Energy Mater.*, 2012, **2**, 873–877.
- 38 H.-G. Wang, Z. Wu, F.-L. Meng, D.-L. Ma, X.-L. Huang, L.-M. Wang and X.-B. Zhang, *ChemSusChem*, 2013, **6**, 56.
- 39 L. J. Fu, K. Tang, K. P. Song, P. A. van Aken, Y. Yu and J. Maier, *Nanoscale*, 2014, **6**, 1384–1389.
- 40 S. Wenzel, T. Hara, J. Janek and P. Adelhelm, *Energy Environ. Sci.*, 2011, **4**, 3342–3345.
- 41 Y. M. Li, L. Q. Mu, Y.-S. Hu, H. Li, L. Q. Chen and X. J. Huang, *Energy Storage Materials*, 2015, doi:10.1016/j.ensm.2015.10.003

ARTICLE

Journal Name

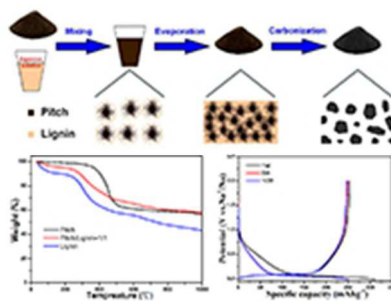
42 L. Qie, W. M. Chen, H. H. Xu, X. Q. Xiong, Y. Jiang, F. Zou, X. L. Hu, Y. Xin, Z. L. Zhang and Y. H. Huang, *Energy Environ. Sci.*, 2013, **6**, 2497–2505.

43 D. A. Stevens and J. R. Dahn, *J. Electrochem. Soc.*, 2000, **147**, 4428–4431.

44 C. Bommier, T. W. Surta, M. Dolgos and X. L. Ji, *Nano Lett.*, 2015,

doi: 10.1021/acs.nanolett.5b01969.

45 Y. M. Li, S. Y. Xu, X. Y. Wu, J. Z. Yu, Y. S. Wang, Y. -S. Hu, H. Li, L. Q. Chen and X. J. Huang, *J. Mater. Chem. A*, 2015, **3**, 71.



53x39mm (96 x 96 DPI)